




Cite this: *J. Mater. Chem. C*, 2025, 13, 14433

Preparation of high-performance blue-red dual-emission carbon dots and their application in light conversion films†

Siyuan Yu,^a Yiyun Song,^a Hongmei Yu,^{*a} Shaoyan Wang^{*a} and Wei Chen^{ib} 

A blue-red dual-emission carbon dot (B/R-CD)-based light conversion film was prepared and applied to improve the photosynthetic efficiency of plants. B/R-CDs were synthesized through a one-step hydrothermal method using acrylic acid and *o*-phenylenediamine and showed distinct emission peaks at 420 nm (blue) and 610 nm (red) under $\lambda_{\text{ex}} = 350$ nm. By integrating the B/R-CDs into a polyvinyl alcohol (PVA) matrix, a high-performance blue-red dual-emission light conversion film was constructed that simultaneously blocks ultraviolet and green light while converting them into photosynthetically active blue and red wavelengths. Compared to conventional single-spectrum-conversion materials, the dual-emission system demonstrated superior performance. The results showed that the 4% B/R-CDs/PVA light conversion film significantly promoted the growth of bok choy, lettuce, and choy sum. Specifically, compared to the control group without the film, the fresh weight of bok choy under the light conversion film increased by 152.73%, carotenoid content increased by 96.00%, and flavonoid content increased by 133.91%. This film also increased the fresh weights of lettuce and choy sum by 143%–160%. This light conversion film demonstrates promising application prospects in crop cultivation, simultaneously addressing light-environment optimization and ecosystem carbon sequestration enhancement through improved photosynthetic quantum yield.

Received 1st April 2025,
Accepted 30th May 2025

DOI: 10.1039/d5tc01374g

rsc.li/materials-c

Introduction

Amidst accelerating global climate change driven by anthropogenic greenhouse gas emissions, searching for effective ways to reduce carbon emissions has become the focus of global attention.¹ Enhancing photosynthetic efficiency is one of the key approaches to achieving carbon reduction goals. A 10% improvement in plant photosynthetic efficiency could significantly increase carbon sequestration capacity, potentially absorbing an additional quarter of global carbon emissions, thereby effectively mitigating the threat of climate change.² Therefore, the optimization of photosynthesis has emerged as a key area of research for enhancing crop yield and quality. Although some achievements have been made in the research of agricultural light conversion film at home and abroad, it still faces many challenges such as high price, unstable performance and unrealized large-scale application.³ Many existing

film materials only have the ability to convert a single spectrum, such as adjusting either blue or red light,⁴ which significantly restricts their wider application and effectiveness in agriculture. Therefore, it is an urgent need to develop multi-spectral control function⁵ and achieve excellent performance and cost control of the light transfer film in order to attain more efficient crop yield and ecological benefits.⁶

Fluorescent CDs, as a new photoconversion material,⁷ have become an ideal choice to improve the performance of photoconversion films due to their adjustable fluorescence properties, excellent luminous stability and non-toxicity.^{8–12} Compared to traditional materials, CDs not only have higher optical efficiency¹³ but also abundant hydrophilic functional groups on their surfaces,^{14–16} such as $-\text{NH}_2$, $-\text{OH}$, and $-\text{COOH}$. These functional groups can form hydrogen bonds with hydrophilic groups in polymer chains,^{17,18} significantly enhancing the mechanical properties of composite materials¹⁹ and greatly improving the physical stability and durability of light conversion films.^{20,21} According to the literature, Barman *et al.* successfully prepared a light conversion film using PVA and nitrogen-doped CDs (N-CDs).²² This film has the ability to convert ultraviolet light (mainly UV-A) into blue light. Cheng *et al.* used PVA, cellulose nanocrystals derived from waste paper (CNC_{paper}), and CDs prepared from CNC_{paper} (CDC_{cellulose}) as

^a School of Chemical Engineering, University of Science and Technology Liaoning, Anshan 114051, People's Republic of China. E-mail: seesea0304@163.com, aswsy@163.com

^b School of CHIPS, Xi'an Jiaotong-Liverpool University, Suzhou 215123, China. E-mail: Wei.Chen03@xjtlu.edu.cn

† Electronic supplementary information (ESI) available. See DOI: <https://doi.org/10.1039/d5tc01374g>



raw materials to successfully fabricate a light conversion film that can efficiently achieve the conversion of ultraviolet light into blue light.²³ Additionally, Zhang *et al.* used spinach as the carbon source and polyvinylpyrrolidone (PVP-K30) and polyethylene glycol (PEG-1000) as encapsulating agents to prepare polymer-encapsulated CDs (CD-PVP and CD-PEG). These were then used as key materials to prepare a light conversion film (LCSHL-PE) with the property of converting ultraviolet light into red light.²⁴ Currently, although numerous studies have been conducted on plastic-CD-based light conversion films, these materials typically only convert ultraviolet light into single blue or red light. While these light conversion materials have application value in specific spectral conversion, their inability to achieve multiple spectrum conversions makes them unsuitable for more complex applications. Wang and others²⁵ used PVA, deep blue-emitting carbon dots, and green/red-emitting rare-earth lanthanide element complexes to prepare a luminescent polymer composite film. Although the addition of rare-earth elements can achieve dual light emission in blue and red, the high cost and complex preparation process of rare-earth elements limit their practical application. Therefore, the development of more economical and simple carbon point based light conversion film has become more possible.

In order to further explore the application of CDs in light conversion films, B/R-CDs were prepared by one step hydrothermal method using acrylic acid and *o*-phenylenediamine as raw materials. B/R-CDs have a small particle size, rich surface groups, and good stability; the raw material is cheap and suitable for large-scale production. After their incorporation into a PVA matrix to form light conversion films,²⁶ fluorescence and UV absorption spectral tests showed that the high-performance light conversion film could effectively block and absorb harmful UV and green light, converting them into blue and red lights that match the absorption spectrum of plants. This light conversion film can optimize the light environment of plants and better meet the needs of plants for photosynthesis, thereby improving the efficiency of photosynthesis and promoting the healthy growth of plants. Particularly under high-intensity light or extreme climatic conditions, this film material can significantly reduce UV damage to plants while providing the optimal spectrum needed for plant growth, boosting crop growth potential. In growth experiments with three types of vegetables, the results indicated that, compared to the no-film group and the pure PVA film group, the light conversion film group significantly promoted vegetable growth and increased nutrient content. Therefore, the B/R-CD-based light conversion film holds significant potential and provides valuable guidance for agricultural applications.

Experimental procedure

Materials

O-Phenylenediamine, acrylic acid, acetone, anhydrous ethanol, and sodium hydroxide were all purchased from China National Pharmaceutical Group Chemical Reagents Co, Ltd (Shenyang,

China). PVA was obtained from Tianjin Huasheng Chemical Reagent Co, Ltd. All reagents were of analytical grade. Ultrapure water (resistivity of 18.2 MΩ cm) was used throughout the experiments.

Characterization

Morphological characterization of the samples was conducted using a high-resolution transmission electron microscope (HRTEM, JEM-2100F, JEOL, Japan). X-ray diffraction (XRD) analysis was performed on an X'pert powder diffractometer (PANalytical B.V., Netherlands). Fourier-transform infrared (FT-IR) spectra were recorded using an EQUINOX55 spectrometer (Bruker Optics GmbH, Germany). X-ray photoelectron spectroscopy (XPS) measurements were carried out with a Thermo Scientific K-Alpha spectrometer (Thermo Fisher Scientific, USA). Fluorescence spectra were acquired using an FS5 fluorescence spectrophotometer (Edinburgh Instruments Ltd, UK). UV-Vis absorption spectra were scanned on a TU-1901 UV-Vis spectrophotometer (Beijing Purkinje General Instrument Co, Ltd, China).

Synthesis of B/R-CDs

0.2000 g of *o*-phenylenediamine and 3 mL of acrylic acid were weighed and dissolved in 10 mL of deionized water, and the resulting solution was transferred to a stainless steel high-pressure reactor with a PTFE liner. The reactor was placed in a constant temperature drying oven and the hydrothermal reaction was carried out at 180 °C for 8 hours. At the end of the reaction, the reactor was naturally cooled to room temperature. After ultrasonication for 10 min, the solution was filtered through a 0.22 μm film and centrifuged at 5000 rpm for 20 min; the centrifuged solution was dialyzed in a 500 Da dialysis bag. The dialysis water was changed every 2 h during the dialysis process until the dialysis water in the beaker was completely clarified. Freeze-drying was performed at −65 °C to obtain pink B/R-CDs powder with a yield of 20.36%. The powder was collected and sealed for storage in a dry place. 10 mg of B/R-CDs powder was used to prepare a solution of 1 mg mL^{−1} and was stored in a refrigerator at 4 °C for the next step (as shown in Fig. 1).

Preparation of B/R-CDs/PVA conversion films

B/R-CDs/PVA conversion films were prepared by solvent casting technology. 1 g of PVA was poured into a small beaker containing 40 mL of deionized water and then heated and stirred at 90 °C for 20 min on a constant temperature magnetic stirrer until the PVA was completely dissolved. Then, B/R-CDs powder

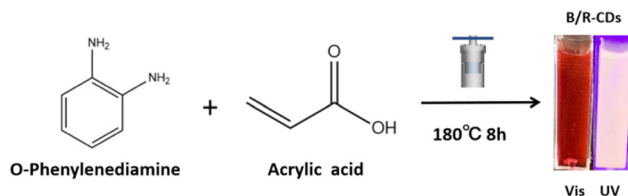


Fig. 1 Schematic diagram of B/R-CDs preparation.



with different qualities was added, and stirring was continued until the B/R-CDs were completely dissolved. The mixture was degassed by ultrasonication for 10 min and poured into the mold, then dried into a film at 50 °C in a constant temperature drying oven. The prepared B/R-CDs/PVA conversion films with ratios of 2%, 3%, 4%, and 5% were then removed for use.

Results and discussion

The morphology and composition of the B/R-CDs were examined utilizing TEM, XRD, FT-IR, and XPS methods. As depicted in Fig. 2a, the HRTEM results reveal that the B/R-CDs are well-dispersed near-spherical nanoparticles. The inset shows clear lattice fringes, with a lattice spacing of approximately 0.21 nm which corresponds to the (100) plane of graphitic carbon.²⁷ The analysis of particle size distribution in Fig. 2b shows that the mean size of the B/R-CDs is 2.03 ± 0.73 nm. The FT-IR analysis (Fig. 2c) suggests that the surface of the B/R-CDs contains an abundance of hydrophilic functional groups. The absorption peak at 3443 cm^{-1} is attributed to the stretching vibrations of O–H/N–H, indicating the presence of hydroxyl and amino groups. The peak at 2952 cm^{-1} corresponds to the stretching vibrations of C–H,²⁸ while the peaks at 1724 cm^{-1} , 1456 cm^{-1} , and 1415 cm^{-1} are attributed to the stretching vibrations of

C=O, C=C, and C–N,²⁹ respectively. Additionally, the peak at 1172 cm^{-1} corresponds to C–O absorption, confirming the B/R-CDs' excellent water solubility. The XRD spectrum of the B/R-CDs is shown in Fig. 2d, where a broad diffraction peak with a peak position at 21.66° indicates that the B/R-CDs are structurally similar to amorphous carbon,³⁰ which confirms the successful synthesis of the B/R-CDs.

To further investigate the chemical structure, elemental chemical states, and composition of the B/R-CDs, XPS analysis was conducted. The XPS survey spectrum (Fig. 3a) reveals that the B/R-CDs are primarily composed of 68.70% C, 1.87% N, and 29.43% O. The C 1s spectrum in Fig. 3b exhibits three peaks at 284.78 eV, 285.18 eV, and 288.88 eV, corresponding to the C–C/
C=C,³¹ C–N/C–O, and C=O bonds, respectively.³² In Fig. 3c, the N 1s spectrum shows two peaks at 399.48 eV and 401.18 eV, corresponding to the C–N and N–H bonds. Lastly, the O 1s spectrum in Fig. 3d reveals two components: C=O at 531.98 eV and C–O at 533.38 eV.³³

The excitation-related optical properties of B/R-CDs were investigated in depth using fluorescence (FL) and UV-visible absorption spectroscopy. As shown in Fig. 4a, the B/R-CDs aqueous solution exhibits three prominent absorption peaks at 206 nm, 271 nm, and 511 nm. The strong absorption at 206 nm can be attributed to the π – π^* transition of C=C double bonds,^{34,35} while the absorptions at 271 nm and 511 nm mainly

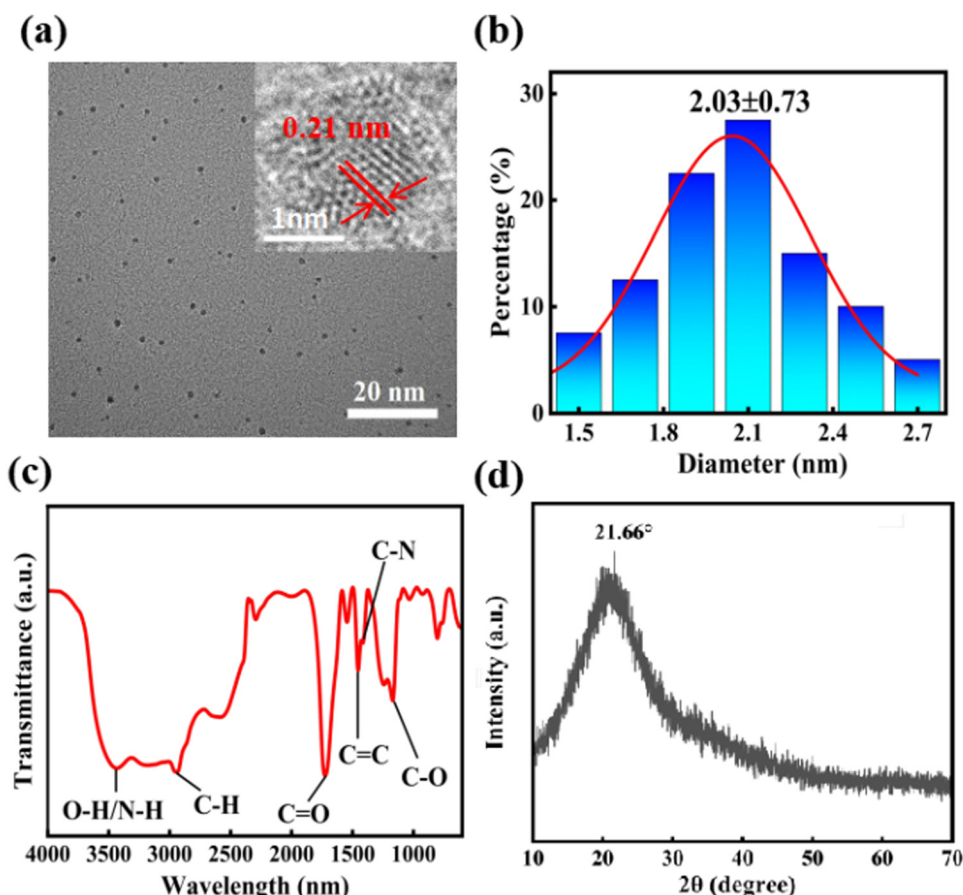


Fig. 2 (a) TEM image of B/R-CDs (inset: The lattice spacing image); (b) particle size distribution diagram; (c) FT-IR spectrum; (d) XRD pattern.



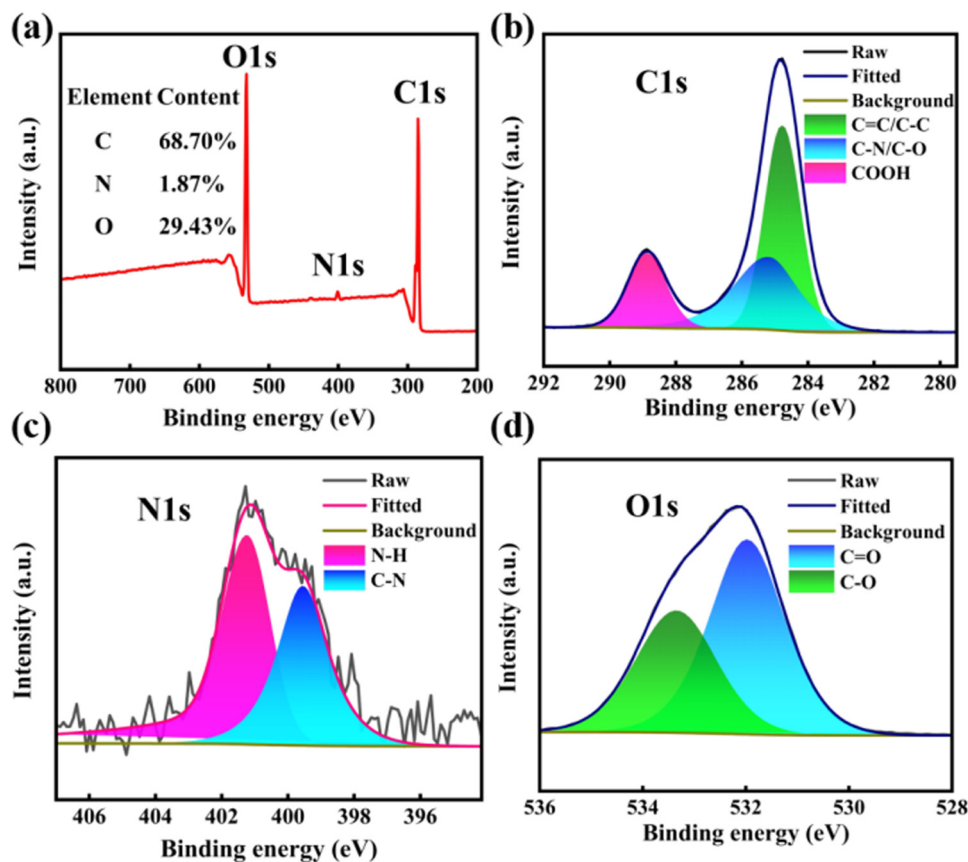


Fig. 3 (a) XPS full spectrum of B/R-CDs; high-resolution spectra of C 1s (b), N 1s (c) and O 1s (d) of B/R-CDs.

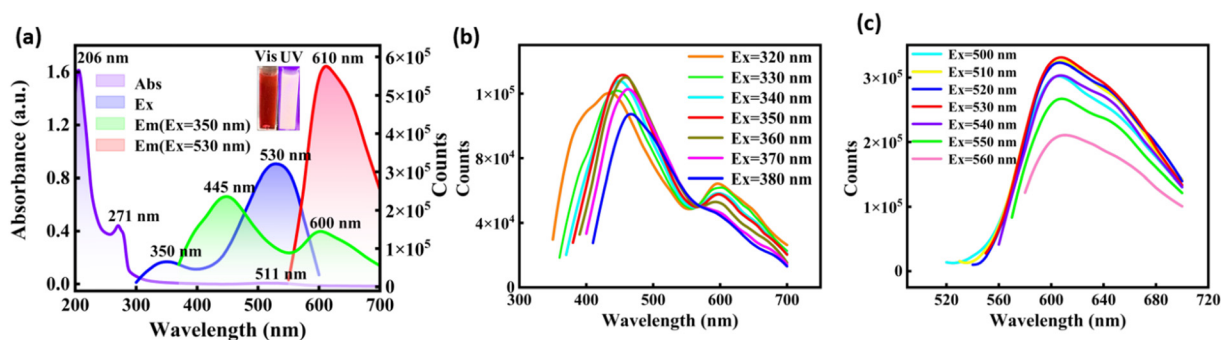


Fig. 4 (a) UV-Vis absorption spectrum and excitation and emission spectra of B/R-CDs. Fluorescence spectra of the B/R-CDs under Ex = 320–380 nm (b) and Ex = 500–560 nm (c).

result from the $n\text{-}\pi^*$ transition of $\text{C}=\text{O}$ bonds³⁶ and the $n\text{-}\pi^*$ transition of $\text{C}=\text{N}$ functional groups on the surface of the B/R-CDs. The inset shows the appearance of the B/R-CDs aqueous solution under visible light and 365 nm UV light. It can be observed that the solution appears red under visible light and emits pink fluorescence when exposed to 365 nm UV light. The excitation spectrum of the B/R-CDs aqueous solution, as shown in Fig. 4a, reveals two main excitation peaks located at 350 nm and 530 nm. The emission spectrum indicates that, under excitation at 350 nm, the emission peaks occur at 445 nm

and 600 nm, while under excitation at 530 nm, the emission peak is at 610 nm. Fig. 4b presents the fluorescence spectrum of B/R-CDs under UV light excitation (320–380 nm, with a 10 nm interval). It can be observed that, as the excitation wavelength increases from 320 nm to 380 nm, the emission wavelength undergoes a red shift, suggesting that the fluorescence properties of the B/R-CDs solution are dependent on the excitation wavelength, exhibiting clear excitation-wavelength-dependent characteristics. Fig. 4c shows the fluorescence spectrum of B/R-CDs under green-to-yellow light excitation



(500–560 nm, spanning the green and partial yellow spectral regions, with 10 nm intervals). As the excitation wavelength increases from 500 nm to 560 nm, a red shift in the emission wavelength is observed, further confirming the influence of excitation wavelength on the fluorescence characteristics of the B/R-CDs solution. To accurately determine the fluorescence quantum yield of the blue-red dual-emission CDs, a relative method was employed for quantitative analysis. Rhodamine 6G³⁷ was used as a reference standard. By plotting the relationship curve between absorbance and fluorescence peak area, the fluorescence quantum yield of these CDs was calculated to be 16.58%.

Under the optimal excitation conditions, the impact of temperature on the fluorescence behavior of the solution was also studied. According to Fig. 5a–c, within the temperature range of 20–80 °C, the fluorescence intensity decreases as the temperature increases, but it recovers to its original intensity upon cooling to room temperature. This indicates that the B/R-CDs solution has good temperature recovery and reversibility,³⁸ suggesting its potential as a temperature sensor and providing a theoretical basis for the fabrication of light conversion films.

The blue-red dual-emission light conversion film was fabricated using the solvent casting technique,³⁹ with varying concentrations of B/R-CDs incorporated into the PVA matrix. Films with concentrations of 2%, 3%, 4%, and 5% were prepared. In order to optimize the concentration of the blue-red dual-emission light conversion film more intuitively, the maximum emission wavelengths of the optimal excitation wavelengths of the light conversion films with 2%, 3%, 4%, and 5% concentrations in the blue light region and the red light region were integrated, as shown in Fig. 6. It can be seen that, when the concentration of the light conversion film was increased from 2% to 4%, the intensity of the dual-emission peaks increased to a certain extent; the fluorescence intensities in the red and blue light regions were maximized simultaneously at a concentration of 4% of the light conversion film. However, when the concentration was further increased to 5%, the fluorescence intensity decreased instead, which might be caused by the concentration quenching effect.⁴⁰ Based on these results, a 4% concentration of the blue-red dual-emission light conversion film was selected as optimal. This concentration-dependent fluorescence

behavior can be attributed to the modulation of the energy transfer efficiency between carbon dots: a moderate increase in the doping concentration facilitates the enhancement of the luminescence center density, whereas too high a concentration leads to a significant enhancement of the non-radiative energy transfer path.

The light conversion film demonstrates three UV absorption peaks at 215 nm, 270 nm, and 540 nm which can be ascribed to the π - π^* transitions of C=C and the n - π^* transitions of C=O in both the light conversion film and the B/R-CDs (Fig. 7a). The diagram also illustrates that the dual-emission light conversion film with 4% B/R-CDs/PVA exhibits two excitation peaks at 330 nm and 530 nm. When excited at 330 nm, it emits at 420 nm and 610 nm, while under excitation at 530 nm, it emits at 610 nm. These emissions fall within the blue and red light regions, which are optimal for plant photosynthesis and closely match the absorption peaks of photosynthetic pigments in these regions. This indicates that the light conversion film can absorb harmful UV and green light and convert them into blue and red light that plants can efficiently absorb, reducing photodamage to plants from high-energy radiation while improving their light energy utilization efficiency. Under sunlight, the light conversion film appears light pink and, under UV lamp illumination, it appears orange-pink (Fig. 7b). Based on the UV transmittance test outcomes of the light conversion film (Fig. 7c), when the amount of CDs added is in the range of 2%–4%, with the increase in B/R-CDs content, the transmittance of the film in the 200–320 nm regions decreases visibly compared to that of the blank film. This demonstrates that increasing the B/R-CDs content enhances the film's ability to block UV light, effectively reducing its harmful effects on plants and promoting plant growth. At the same time, the visible light transmittance increases in the wavelength ranges of 380–480 nm and 570–800 nm. When the doping concentration of CDs reaches 5%, the transmittance across the entire wavelength range shows a significant decrease. Mechanistically, this phenomenon can be attributed, in part, to the concentration quenching effect of CDs. As the concentration of CDs increases substantially, the internal energy transfer processes are altered, and the probability of non-radiative transitions increases significantly. This, in turn, reduces the fluorescence emission efficiency, ultimately leading to a decrease in transmittance.

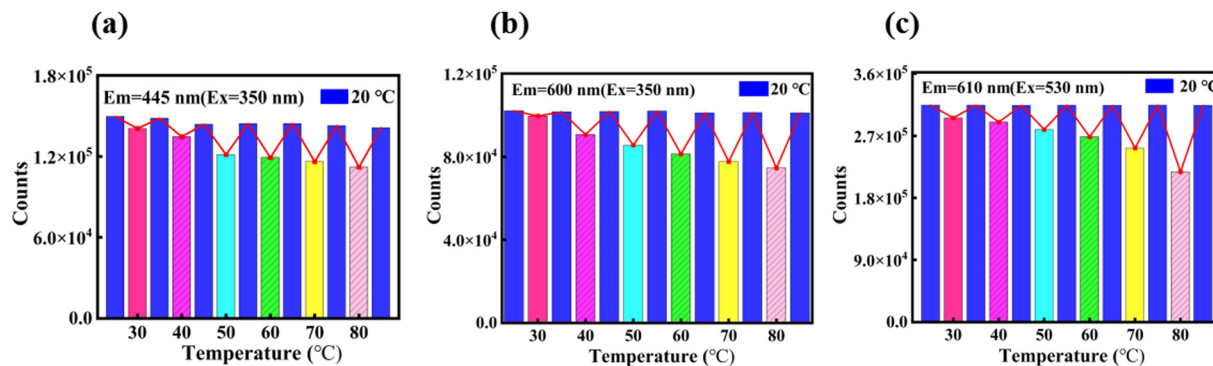


Fig. 5 (a–c) Effect of temperature on the fluorescence intensity at three emission wavelengths of the B/R-CDs light conversion film.



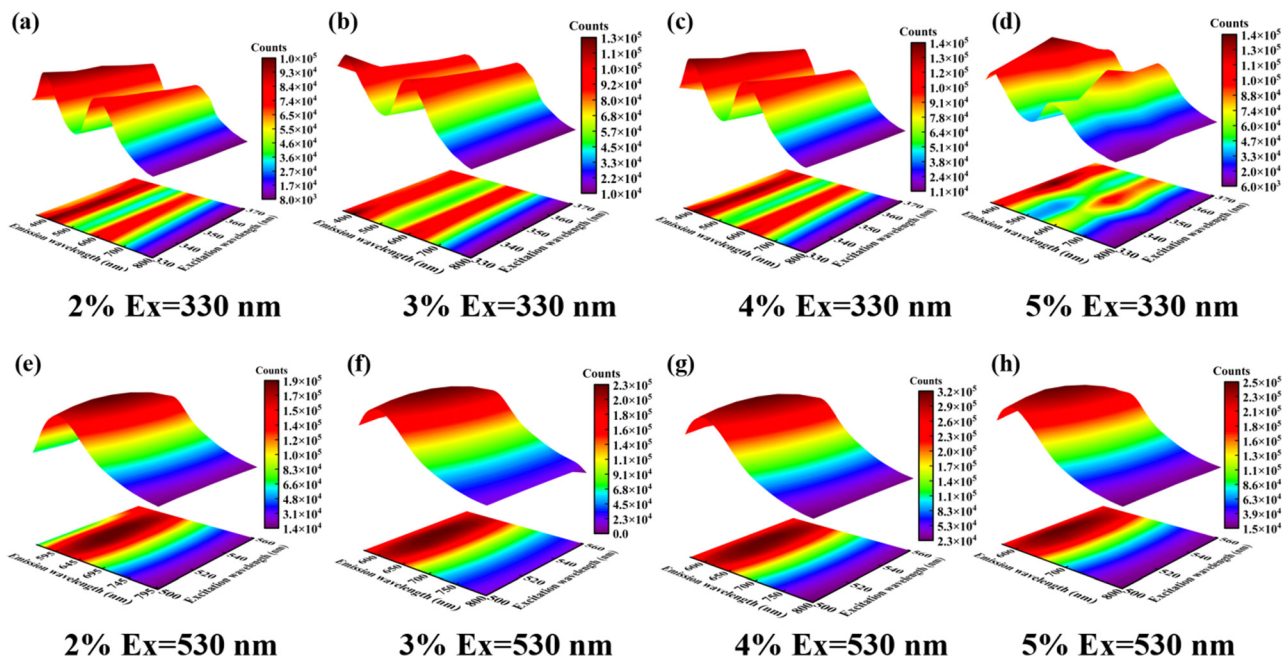


Fig. 6 3D projection fluorescence spectra of the light conversion films with B/R-CDs contents of (a, e) 2%, (b, f) 3%, (c, g) 4%, and (d, h) 5%.

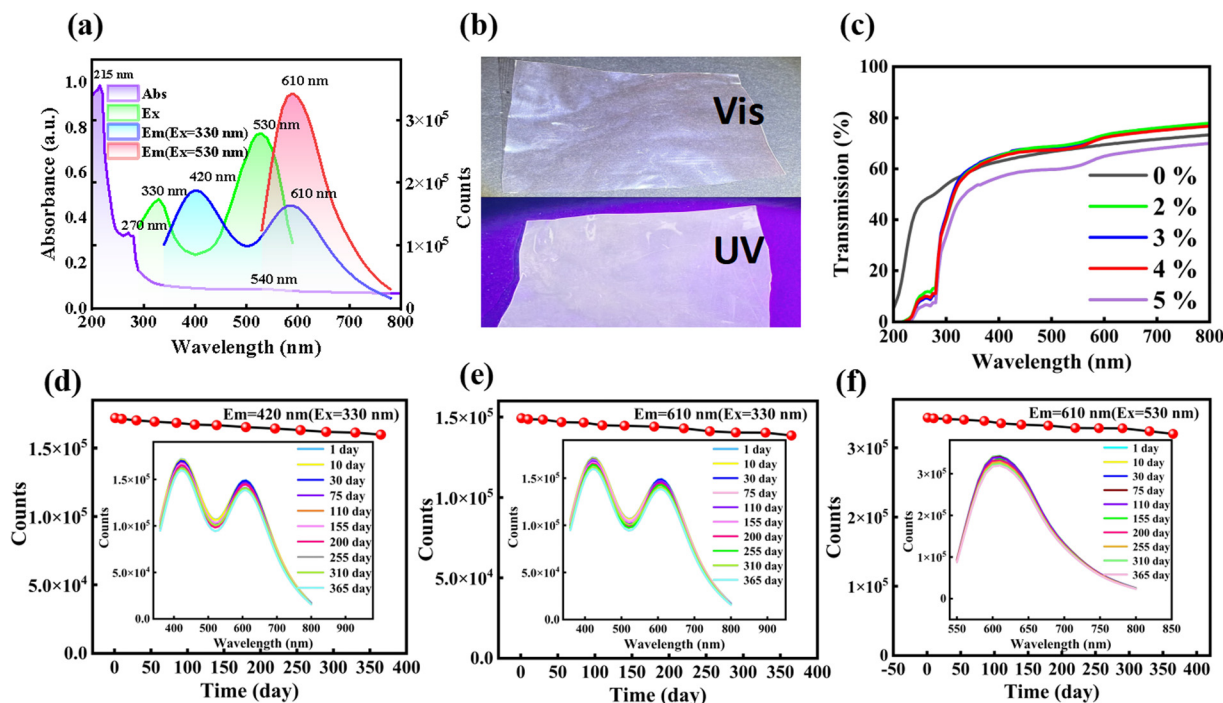
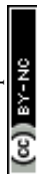


Fig. 7 (a) UV-Vis absorption, excitation, and emission spectra of B/R-CDs/PVA film. (b) Physical image of the 4% B/R-CDs/PVA film under natural and UV light. (c) UV transmittance of films with different B/R-CDs concentrations. (d)–(f) Effect of storage time on fluorescence intensity at three emission wavelengths.

To further investigate the stability of the light conversion performance of the B/R-CDs light conversion film, we conducted a tracking test on the fluorescence intensity changes of the film over time (Fig. 7d–f). Experimental data record the

fluorescence intensity variation over a 365-day period. The findings indicate that the fluorescence strength of the film decreased progressively over time. By the end of the 365-day observation period, there was an approximate 7% decrease in



fluorescence intensity. This suggests that the light conversion film retains strong performance over one year. In general, the light conversion film exhibits exceptional fluorescence stability during prolonged storage, highlighting its impressive long-term stability in light conversion properties. Additionally, we measured the quantum yield of the B/R-CDs/PVA light conversion film to be 34.32%. The increase in the PLQY value of the light conversion film is due to the synergistic effect between the B/R-CDs and the PVA matrix. This synergistic effect optimizes the light conversion process, reduces energy loss, enables more absorbed light energy to be emitted in the form of fluorescence, and thus increases the PLQY value of the light conversion film.

To investigate the impact of B/R-CDs introduction on the surface morphology of the PVA film, SEM analysis was conducted on both the pure PVA film and the 4% B/R-CDs/PVA light conversion film. As depicted in Fig. 8a, the surface of the pure PVA film appears smooth with some small granular protrusions. However, the addition of B/R-CDs leads to a significant transformation in the surface morphology of the B/R-CDs/PVA light conversion film, as shown in Fig. 8b, with the granular projections being replaced by larger blocky shapes and a substantial increase in surface roughness. This observation suggests a drastic alteration in the surface morphology characteristics of the PVA film due to the presence of B/R-CDs. Additionally, AFM analysis was carried out to quantitatively assess the change in surface roughness. Fig. 8c presents the AFM image of the pure PVA film, revealing an average roughness (R_a) and root-mean-square roughness (R_q) of 4.27 nm and 6.24 nm, respectively. Fig. 8d shows the AFM image of

the B/R-CDs/PVA light conversion film, with a mean roughness (R_a) and root-mean-square roughness (R_q) of 25.9 nm and 35.3 nm, respectively. The mean roughness and root-mean-square roughness of the B/R-CDs/PVA light conversion film were found to increase by 21.63 nm and 29.06 nm, respectively, in comparison to the pure PVA film. This consistency with the SEM findings further confirms the successful incorporation of B/R-CDs into the PVA substrate and the successful preparation of conversion films. Fig. 8e and f demonstrate the correlation between the content of B/R-CDs and the tensile strength of the B/R-CDs/PVA light conversion film. It is evident that, as the content of B/R-CDs increases, both the thickness and tensile strength of the film gradually increase, reaching a maximum tensile strength of 51.45 MPa at a B/R-CDs content of 4%, which is 17.65 Mpa higher than that of pure PVA film. However, when the B/R-CDs content reaches 5%, the tensile strength decreases to 41.15 Mpa. The observed outcome can be ascribed to the saturation of B/R-CDs within the PVA matrix, leading to the aggregation of excess B/R-CDs and subsequently impacting the structure of the light conversion film, resulting in a decrease in the tensile strength of the composite film.

We delved deeper into the light conversion mechanism of the blue-red dual-emission light conversion film, as shown in Fig. 9. Our analysis of the B/R-CDs using FT-IR and XPS revealed that they are predominantly made up of carbon, oxygen, and a minor amount of nitrogen, with these elements primarily existing in the form of C=C, C=O/C-O, C-N/N-H functional groups. These functional moieties play a crucial role in the fluorescence production of B/R-CDs. Through analyses of UV-visible absorption and fluorescence spectra, the UV absorption spectrum of the B/R-CDs solution was found to closely coincide with its fluorescence spectrum. Upon UV excitation, electrons are initially elevated to the π^* state in the carbon core, followed by vibrational relaxation through interaction with the LUMO of the surface states, influenced by nitrogen and oxygen-functional groups.^{41,42} The presence of oxygen and nitrogen groups introduces new energy levels, effectively reducing the energy gap between the LUMO and HOMO of the surface states. Ultimately, fluorescence emission occurs as the electrons

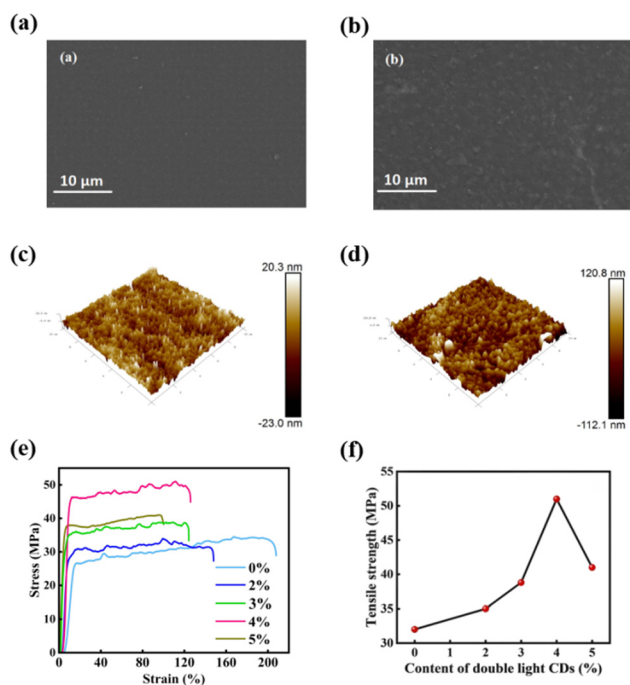


Fig. 8 (a) SEM of the PVA film; (b) SEM of 4% B/R-CDs/PVA film; (c) AFM of PVA film; (d) AFM of 4% B/R-CDs/PVA film; (e) stress-strain curves of B/R-CDs/PVA film; (f) relationship between the B/R-CDs content and tensile strength.

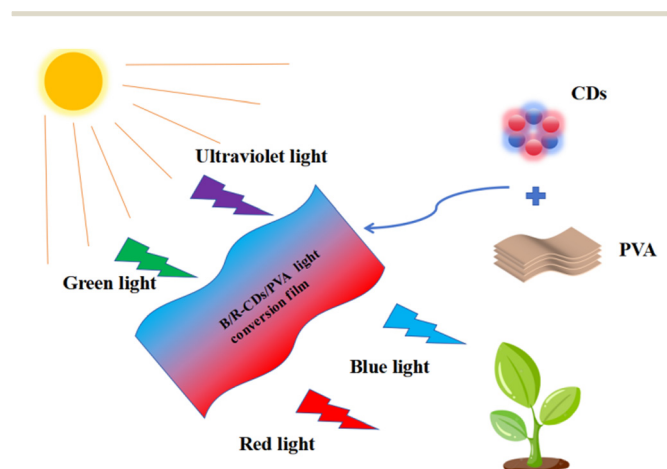


Fig. 9 Light conversion mechanism diagram.



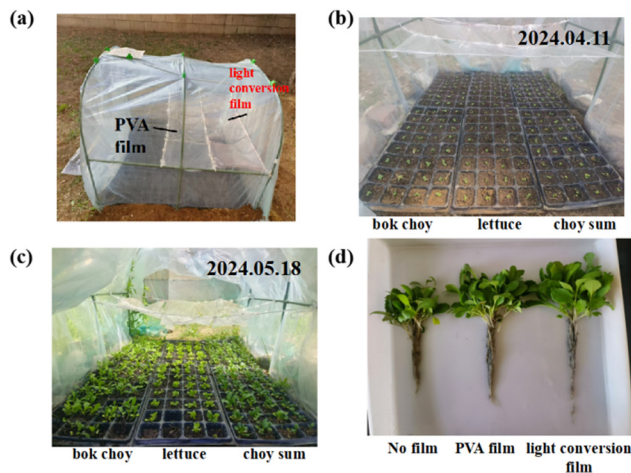


Fig. 10 (a) Simulated greenhouse diagram; (b) and (c) growth process images of bok choy, lettuce, and choy sum; (d) height comparison of bok choy.

recombine radiatively and revert back to the HOMO of the surface states. When combined with polyvinyl PVA to create a light conversion film, the B/R-CDs and PVA are securely bonded through hydrogen bonds. The composite film draws on the fluorescence emission of the B/R-CDs to produce blue and red fluorescence under excitation by UV and green light, respectively. When applied to crop cultivation, this light conversion film can convert light into the energy required by plants, promoting their growth. Specifically, during the fluorescence emission process, the energy difference generated is released in the form of internal energy, which raises the surrounding temperature, thus accelerating the germination of crop seeds. Once the seeds start to sprout and the leaves start to emerge, the pigment molecules in the leaves, which have rich conjugated structures, are stimulated by the light absorbed by the film. The electrons within the conjugated structure are energized from their original state to an excited state, initiating the transfer of electrons and protons. This process not only enhances light absorption and energy transfer but also improves the plant's light absorption efficiency, further promoting plant growth and development. In summary, the carbon dot light conversion film, through its unique light conversion and energy

release mechanisms, not only enhances the light absorption capacity of plants but also effectively promotes crop growth, demonstrating significant potential for agricultural applications.

We constructed an outdoor greenhouse (Fig. 10a) for the experiment, with the test crops being bok choy, lettuce, and choy sum. The experimental cover films used were light conversion films with a 4% carbon dot content, PVA films, and non-cover films (from inside to outside, Fig. 10b and c). Three groups of experiments were set up, and the cultivation lasted for 45 days. Taking bok choy as an example, the images from left to right show bok choy grown under no film, PVA film, and dual-emission carbon dot light conversion film (Fig. 10d). We measured the plant height, root length, stem length, leaf length, and leaf width of all germinated bok choy and recorded the average values. We weighed the fresh and dry weights of 25 bok choy plants and obtained the average value through multiple measurements. The germination rate of bok choy, the above-mentioned morphological indices, and the fresh and dry weights are summarized in Table 1. The photosynthetic pigment content is recorded in Table 2, and the nutrient element content is recorded in Table 3. It is evident that bok choy grew best under the carbon dot light conversion film. Fig. S1 in ESI† presents the plant height comparison of lettuce, while Tables S1–S3 in ESI† compare various indicators of lettuce. Fig. S2 in ESI† shows the plant height comparison of choy sum, and Tables S4–S6 in ESI† compare the growth indicators of choy sum. It can be seen from the ESI† that both lettuce and choy sum showed the best growth state under the treatment of carbon dot light conversion film. Compared with the no-film group, the fresh weight of lettuce increased by 143.9%; the fresh weight of choy sum increased by 160.7%. In addition, the germination rate, plant height, root development, photosynthetic pigments and nutrient contents in the light conversion film treatment group were significantly higher than those in the control group.

The dual-emission light conversion film significantly enhanced the growth and nutritional content of bok choy. Compared to the no-film group, the fresh weight increased by 152.73%, carotenoid content increased by 96.00%, and flavonoid content increased by 133.91%. Compared to the pure PVA film group, the dual-emission light conversion film led

Table 1 Effect of light conversion film with 4% carbon dot content on the growth and development of bok choy

Experimental group	Germination rate (%)	Plant height (cm)	Fresh weight (g)	Dry weight (g)	Root length (cm)	Blade length (cm)	Blade width (cm)
No film	85	6.06 ± 0.42	1.244 ± 0.12	0.124 ± 0.01	8.76 ± 0.71	2.86 ± 0.33	1.52 ± 0.19
PVA film	92.50	6.96 ± 0.34	2.324 ± 0.23	0.18 ± 0.02	11.32 ± 0.73	4.12 ± 0.43	1.91 ± 0.18
Light conversion film	98.75	8.53 ± 0.54	3.144 ± 0.21	0.228 ± 0.01	13.07 ± 1.32	5.12 ± 0.21	2.38 ± 0.26

Table 2 Effect of light conversion film with 4% carbon dot content on photosynthetic pigment contents in bok choy

Experimental group	Chlorophyll a (mg g ⁻¹)	Chlorophyll b (mg g ⁻¹)	Chlorophyll a + b (mg g ⁻¹)	Carotenoids (mg g ⁻¹)
No film	0.117 ± 0.01	0.036 ± 0.02	0.153 ± 0.02	0.075 ± 0.02
PVA film	0.129 ± 0.02	0.039 ± 0.02	0.168 ± 0.01	0.110 ± 0.01
Light conversion film	0.211 ± 0.02	0.041 ± 0.01	0.252 ± 0.01	0.147 ± 0.03



Table 3 Effect of light conversion film with 4% carbon dot content on nutrient contents of bok choy

Experimental group	Soluble protein (mg g ⁻¹)	Vitamin C (mg g ⁻¹)	Soluble sugar (mg g ⁻¹)	Polyphenol (mg g ⁻¹)	Flavonoid (mg g ⁻¹)
No film	0.667 ± 0.01	0.133 ± 0.01	0.036 ± 0.01	0.143 ± 0.01	0.874 ± 0.01
PVA film	0.706 ± 0.01	0.148 ± 0.02	0.039 ± 0.01	0.183 ± 0.01	1.305 ± 0.01
Light conversion film	0.811 ± 0.01	0.166 ± 0.02	0.041 ± 0.01	0.213 ± 0.01	2.042 ± 0.02

to a 35.28% increase in fresh weight, a 63.56% increase in chlorophyll a content, and a 56.48% increase in flavonoid content. It also significantly improved key nutrients such as vitamin C and soluble proteins. These substantial improvements indicate that the blue-red dual-emission light conversion film optimizes the spectral distribution and enhances the plant's absorption efficiency of red and blue light, thereby increasing light energy utilization during photosynthesis and ultimately promoting comprehensive growth and quality improvement of plants.

Conclusions

In summary, we synthesized high-performance blue-red dual-emission B/R-CDs with a yield of 20.36% using a simple one-pot hydrothermal method and successfully applied them to the preparation of light conversion films. The B/R-CDs have small particle sizes, abundant surface functional groups, and good stability, effectively converting UV and green light into the blue and red light required by plants. By combining the CDs with PVA, the resulting light conversion films can precisely adjust the light spectrum, optimize the plant growth environment, improve crop photosynthesis efficiency, and promote healthy plant growth. In practical applications, the light conversion films show significant advantages in promoting vegetable growth, increasing nutrient content, and improving photosynthetic pigment synthesis, providing important experimental evidence and application prospects for agricultural light conversion film research and promotion.

Author contributions

Siyuan Yu and Yiyun Song: experimental design, synthesis and characterization; Siyuan Yu, Hongmei Yu: data analysis, editing and polishing; Hongmei Yu, Shaoyan Wang and Wei Chen: conceptualization, experimental design, supervision, editing and funding.

Data availability

All data will be available and provided by the authors upon request.

Conflicts of interest

The authors declare no conflicts of interest.

Acknowledgements

This work was supported by XingLiao Talent Project Grants (No. XLYC1902076), the XJTLU Research Development Funding (RDF-21-01-027, RDF-24-01-037), the Jiangsu Department of Education Funding for the School of CHIPS at XJTLU (EFP10120240023, EFP10120240024).

References

- 1 J. Flexas and M. Carriqui, *Plant J.*, 2020, **101**, 964–978.
- 2 A. Sela, U. Piskurewicz, C. Megies, L. Mène-Saffrané, G. Finazzi and L. Lopez-Molina, *Plant Physiol.*, 2020, **182**, 2166–2181.
- 3 J. Wang, X. Qiao, B. Li, B. Liu, J. Zhang, Z. Yan, P. Hao, X. Wang, Y. Liu, L. Shen and Z. Wang, *Heliyon*, 2024, **10**, e36967.
- 4 Y. Yu, Y. Wang, W. Liu, X. Jia, L. Ma, L. Ren, M. Xue and X. Liu, *Dyes Pigm.*, 2018, **159**, 483–490.
- 5 Y. Fan, Y. Zhou, Z. Qiu and S. Lian, *J. Mater. Chem. C*, 2025, **13**, 5462–5482.
- 6 Y. Liu, Z. Gui and J. Liu, *Polymers*, 2022, **14**, 851.
- 7 J. Liu, R. Li and B. Yang, *ACS Cent. Sci.*, 2020, **6**, 2179–2195.
- 8 M. Jiang, Y. Sun, M. Chen, H. Ji, Y. Liu, R. Qin, X. Li, H. Gao, R. Zhang and L. Zhang, *Chem. Eng. J.*, 2024, 153761.
- 9 X. Tang, H. Yu, B. Bui, L. Wang, C. Xing, S. Wang, M. Chen, Z. Hu and W. Chen, *Bioact. Mater.*, 2021, **6**, 1541–1554.
- 10 H. Liu, Z. Xie and M. Zheng, *Small*, 2023, **19**, 2206683.
- 11 Y. Xu, H. Yu, L. Chudal, N. Pandey, E. Amador, B. Bui, L. Wang, X. Ma, S. Deng, X. Zhu, S. Wang and W. Chen, *Mater. Today Phys.*, 2021, **17**, 100328.
- 12 M. Zhan, H. Yu, L. Li, D. Nguyen and W. Chen, *Anal. Chem.*, 2019, **91**, 2058–2065.
- 13 Z. Wei, W. Lu, X. Wang, J. Ni, U. Prova, C. Wang and G. Huang, *J. Mater. Chem. C*, 2022, **10**, 1932–1967.
- 14 X. Xu, Y. Li, G. Hu, L. Mo, M. Zheng, B. Lei, X. Zhang, C. Hu, J. Zhuang and Y. Liu, *J. Mater. Chem. C*, 2020, **8**, 16282–16294.
- 15 T. Medeiros, J. Manioudakis, F. Noun, J. Macairan, F. Victoria and R. Naccache, *J. Mater. Chem. C*, 2019, **7**, 7175–7195.
- 16 R. Cheng, T. Zhang, X. Huang and J. Yu, *Chin. Chem. Lett.*, 2024, **35**, 108763.
- 17 X. Tang, H. Wang, H. Yu, B. Bui, W. Zhang, S. Wang, M. Chen, L. Yuan, Z. Hu and W. Chen, *Mater. Today Phys.*, 2022, **22**, 100576.
- 18 J. Yang, L. Guo, X. Yong, T. Zhang, B. Wang, H. Song, Y. Zhao, H. Hou, B. Yang, J. Ding and S. Lu, *Angew. Chem., Int. Ed.*, 2022, **61**, e202207817.
- 19 J. You, S. Chen and Y. Wang, *Chin. Chem. Lett.*, 2017, **28**, 201–205.



- 20 B. Fu, Q. Liu, M. Liu, X. Chen, H. Lin, Z. Zheng, J. Zhu, C. Dai, X. Dong and D. Yang, *Chin. Chem. Lett.*, 2022, **33**, 4577–4582.
- 21 Y. You, H. Zhang, Y. Liu and B. Lei, *Carbohydr. Polym.*, 2016, **151**, 245–250.
- 22 B. Barman, T. Nagao and K. Nanda, *Appl. Surf. Sci.*, 2020, **510**, 145405.
- 23 X. Cheng, Q. Zhao, J. Kang, X. Zhao, X. He and J. Li, *ACS Appl. Polym. Mater.*, 2023, **5**, 6307–6317.
- 24 S. Zhang and J. He, *J. Mater. Chem. A*, 2024, **12**, 2070–2080.
- 25 Y. Wang, K. Čépe and R. Zbořil, *J. Mater. Chem. C*, 2016, **4**, 7253–7259.
- 26 T. Li, Y. Zheng, C. Wu, C. Yan, C. Zhang, H. Gao, Q. Chen and K. Zhang, *Chin. Chem. Lett.*, 2022, **33**, 4238–4242.
- 27 C. Liu, R. Cheng, J. Guo, G. Li, H. Li, H. Ye, Z. Liang, C. Wang and S. Chen, *Chin. Chem. Lett.*, 2022, **33**, 304–307.
- 28 L. Zhou, H. Wang, H. Yu, E. Amador, J. Xue, S. Wang and W. Chen, *J. Mater. Chem. C*, 2023, **11**, 15926–15933.
- 29 T. Habteyes, E. Westphal, K. Plackowski, P. Kotula, M. Meyerson, S. White, W. Corbin, K. Ghosh and J. Grey, *Nano Lett.*, 2023, **23**, 9474–9481.
- 30 Y. Liu, N. Xiao, N. Gong, H. Wang, X. Shi, W. Gu and L. Ye, *Carbon*, 2014, **68**, 258–264.
- 31 X. Wang, P. Yang, Q. Feng, T. Meng, J. Wei, C. Xu and J. Han, *Polymers*, 2019, **11**, 616.
- 32 X. Yang, L. Sui, B. Wang, Y. Zhang, Z. Tang, B. Yang and S. Lu, *Sci. China Chem.*, 2021, **64**, 1–7.
- 33 G. Hu, Y. Wang, S. Zhang, H. Ding, Z. Zhou, J. Wei, X. Li and H. Xiong, *Carbon*, 2023, **203**, 1–10.
- 34 P. He, J. Bai, F. Qin, X. Wang, X. Yu, Y. Yao and L. Ren, *Appl. Surf. Sci.*, 2024, **652**, 159367.
- 35 C. Ji, Q. Han, Y. Zhou, J. Wu, W. Shi, L. Gao, R. Leblanc and Z. Peng, *Carbon*, 2022, **192**, 198–208.
- 36 X. Zhang, Y. K. Ren, Z. Ji and J. Fan, *J. Mol. Liq.*, 2020, **311**, 113278.
- 37 X. Yang, Q. Li, M. Tang, Y. Yang, W. Yang, J. Hu, X. Pu, J. Liu, J. Zhao and Z. Zhang, *ACS Appl. Mater. Interfaces*, 2020, **12**, 20849–20858.
- 38 H. Zhang, J. You, J. Wang, X. Dong, R. Guan and D. Cao, *Dyes Pigm.*, 2020, **173**, 107950.
- 39 M. Suhasini, K. Rajeshwari, S. Bindya, A. Hemavathi, V. Prashant, S. Asad, E. Rajalakshmanan, A. Raghavendra, S. Chandan, C. Kumar, M. Sanjay and K. Prasad, *Heliyon*, 2023, **9**, e15792.
- 40 Y. Ru, G. I. N. Waterhouse and S. Lu, *Aggregate*, 2022, **3**, e296.
- 41 B. Zhang, G. An, J. Chen, H. Guo and L. Wang, *J. Colloid Interface Sci.*, 2023, **637**, 173–181.
- 42 H. Wang, P. Haydel, N. Sui, L. Wang, Y. Liang and W. Yu, *Nano Res.*, 2020, **13**, 2492–2499.

